Journal of Power Sources 211 (2012) 177–183

Contents lists available at SciVerse ScienceDirect

Journal of Power Sources

journal homepage: www.elsevier.com/locate/jpowsour

Cr-poisoning in (La,Sr)(Co,Fe)O_3 cathodes after 10,000 h SOFC stack testing

J. Andreas Schuler [a,b,c,*], Zacharie Wuillemin [d], Aïcha Hessler-Wyser [b], Clément Comminges [e,1], Nadia Yousfi Steiner [e], Jan Van herle [a]

[a] Industrial Energy Systems Laboratory (LENI), Ecole Polytechnique Fédérale (EPFL), CH-1015 Lausanne, Switzerland
[b] Interdisciplinary Center for Electron Microscopy (CIME), Ecole Polytechnique Fédérale (EPFL), CH-1015 Lausanne, Switzerland
[c] Laboratory for High Performance Ceramics (HPC), Swiss Federal Laboratories for Materials Science and Technology (EMPA), CH-8600 Dübendorf, Switzerland
[d] HTceramix, CH-1400 Yverdon, Switzerland
[e] European Institute For Energy Research (EIFER), 73131 Karlsruhe, Germany

ARTICLE INFO

Article history:
Received 30 December 2011
Received in revised form
24 February 2012
Accepted 24 March 2012
Available online 10 April 2012

Keywords:
Solid oxide fuel cells (SOFC)
Cathode
Cr-poisoning
Sealing

ABSTRACT

After 10,000 h solid oxide fuel cell (SOFC) stack operation, the Cr-poisoning situation in $(La_{0.6}Sr_{0.4})(Co_{0.2}Fe_{0.8})O_3$ (LSCF)-based cathode material is depicted in this work. Systematic Cr profiling by energy-dispersive X-ray spectroscopy (EDS), from post-operation samples taken at different locations within the air flow field, reveals Cr accumulation in electrochemically active cathode regions, although the major amount of Cr is trapped in inactive surface-proximal cathode regions; the 20 m LSCF current collector does not fully impede the Cr access to the functional cathode.

The distribution of Cr within the flow field reports on the severity of the sources and causes for Cr contamination: 1) Cr preferentially accumulates at sealing-proximal locations; this is explained by fuel-leakage through the sealing with subsequent water vapor generation in the cathode compartment, aggravating local Cr-poisoning via the Cr-oxyhydroxide vapor species; 2) high Cr amounts at air inlet regions point to system components located upstream of the cell to contribute to local Cr contamination; 3) the remaining main part of the cell experiences low Cr-poisoning; the protective solution to prevent Cr evaporation from the metallic interconnects thus appears to be adequate.

The detected low overall amounts of Cr contamination, partially correlated to the observed low performance degradation, encouragingly indicate 40,000 h operation, a prerequisite for stationary SOFC application, to be in reach for LSCF-based stacks.

1. Introduction

The market entry for solid oxide fuel cells (SOFC) as stationary application is promised for SOFC systems reaching reliably a life-span of 40,000 h. As such a time span precludes repetitive testing in small scale SOFC development programs, 10,000 h benchmarking with low and stable degradation rates and without major incidents meets a first important step. In this context, the present work aims to depict the severity of degradation effects after such endurance testing, based on the post-test analysis of SOFC stack components, to forecast the device behavior at longer operating time.

The stack test dealt with in this study, a 5-cell short-stack with cell design and characteristics depicted in Fig. 1, was operated over 9630 h at 750 °C under a constant current load of 0.5 A cm^{-2} (25 A for the whole stack), with simulated reformate gas at a fuel utilization of 73%. Comminges et al. monitored, via impedance spectroscopy, the stack performance and degradation evolution over the complete testing time [1] (cf. Figs. 2 and 3) and recorded a stack potential decay from 3.752 V to 3.241 V, which represents 13.6% total degradation over ca. 10,000 h, caused by an area specific resistance (ASR) increase of 0.2 Ω cm^2 that could be attributed to 0.18 Ω cm^2 ohmic resistance increase and 0.02 Ω cm^2 polarization resistance increase.

As only few stack tests, comprising $(La_{0.6}Sr_{0.4})(Co_{0.2}Fe_{0.8})O_3$ (LSCF)-based cathode materials, having reached the milestone of 10,000 h lifetime, with subsequent post-test analysis, are reported in open literature [2], focus is brought here to the cathodic half-cell, i.e. cathode regions from the electrolyte to the current collector toward the metallic interconnector (MIC).

* Corresponding author. Industrial Energy Systems Laboratory (LENI), Ecole Polytechnique Fédérale (EPFL), CH-1015 Lausanne, Switzerland. Tel.: +41 (0)21 693 4827; fax: +41 (0)21 693 3502.
E-mail address: andreas.schuler@epfl.ch (J.A. Schuler).
[1] Current address: Institut für Biochemie und Biologie, AG Molekulare Enzymologie, Universität Potsdam, 14476 Golm, Germany.

0378-7753/$ – see front matter © 2012 Elsevier B.V. All rights reserved.
doi:10.1016/j.jpowsour.2012.03.045

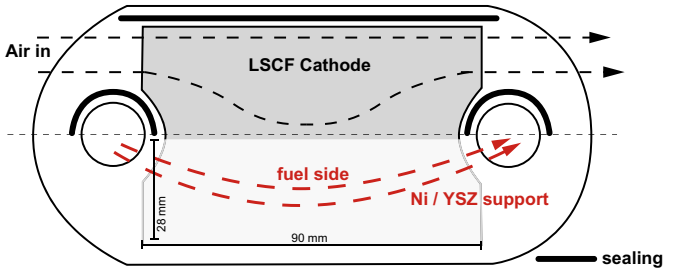

Fig. 1. Design of the anode-supported Ni-YSZ cell with an LSCF-based cathode where the air and fuel flow fields are schematically indicated.

Since the test was performed in stack configuration, the compatibility between stack/system compounds and the air electrode needs investigation. In particular, emanation of volatile $Cr^{(VI)}_{(g)}$ species from Cr-containing alloys, present in MIC and system components, such as tubing, heating and housing elements, is expected [3–5]. The Cr-poisoning degradation phenomenon is therefore suspected to occur via the accumulation of reduced $Cr^{(III)}_{(s)}$ in cathode layers, blocking gaseous and electric paths necessary for the cathode oxygen reduction reaction, leading to performance degradation over time [6]. The quantity of emanated Cr species strongly depends on the partial water vapor pressure, as volatile Cr-oxyhydroxide $CrO_2(OH)_{2(g)}$ generation is directly proportional to the local $p(H_2O)$ [6].

Hydrogen leakage through sealing materials with subsequent water generation in the cathode compartment has been pointed out by Wuillemin et al. [7]. They made a model prediction of the distribution of the local water vapor pressure for the cell design dealt with in this work, depicted in Fig. 4. Coupling thermodynamic data for Cr vapor species to the local conditions in the cathode compartment enabled to predict the local concentrations of generated Cr [8], and therefore to point out regions more or less prone to Cr-poisoning. The Cr vapor generation modeling result will be illustrated in Fig. 9[B].

The combination of these modeling results, used as guidelines for sample location choice for post-operation analysis (indicating the so-called compound formation area [9] between LSCF and Cr),

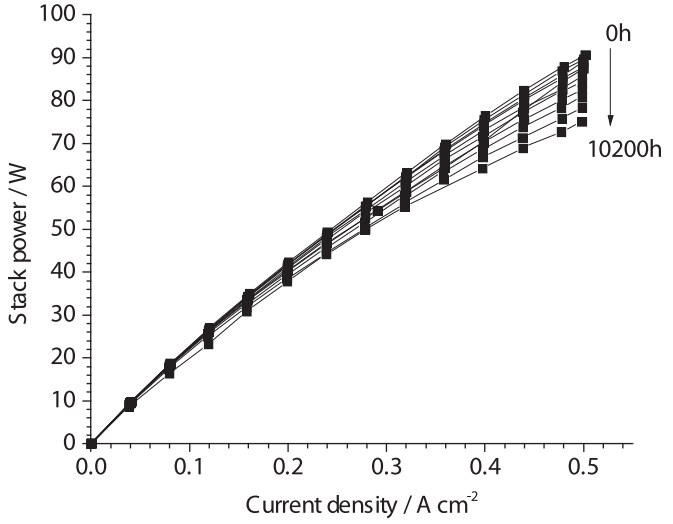

Fig. 2. Stack output power versus time and current density; the stack power decreased from 91 W to 75 W (ca. 18% decrease) after 10,200 h operation. Reprinted with permission from Ref. [1].

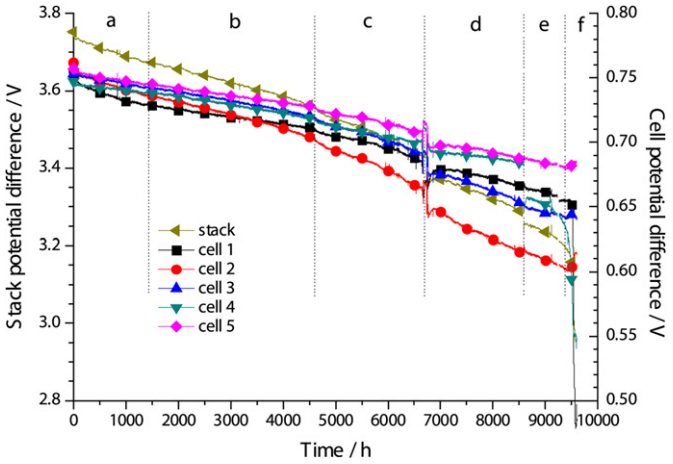

Fig. 3. Stack and cells voltages versus time; annotations a–f correspond to 6 different degradation domains; regions a and b result from steady-state operation; domains c, d and e are accelerated domains initiated by testing setup failures reported in Table 2. Reprinted with permission from Ref. [1].

and the corresponding electrochemical behavior evolution is the starting point of this study.

We aim to picture the Cr-poisoning situation after 10,000 h endurance testing of an LSCF cathode-based SOFC stack. Judged on both the severity and distribution of Cr accumulations in the cathode compartment, we intend to shed light on the causes and sources of Cr-poisoning, and so to suggest solutions to mitigate Cr-poisoning for the extension to 40,000 h lifetime for LSCF-based SOFC stacks.

2. Experimental

The 5-cell stack test with 50 cm^2 active area per cell as illustrated on Fig. 1, provided by *SOFCPower/HTceramix*, comprises $(ZrO_2)_{0.92}(Y_2O_3)_{0.08}$ (YSZ) electrolyte-covered Ni-YSZ anode-supported cells with a $(Ce_{0.9}Gd_{0.1})O_{1.95}$ (CGO) barrier layer toward the $(La_{0.6}Sr_{0.4})(Co_{0.2}Fe_{0.8})O_3$-based CGO–LSCF composite cathode, an LSCF current collector layer, a *CROFER22APU* (*ThyssenKrupp*) metallic interconnect covered with a $(MnCo_{1.9}Fe_{0.1})O_4$ protective coating and using the proprietary material *SOFConnex*™ as gas diffusion layer (GDL).

The stack performance and degradation evolution, as previously reported [1], is summarized in Table 1 and illustrated in Figs. 2 and 3.

The degradation rate during the first 5000 h was about 1% per 1000 h, but increased afterward above 1.5% per 1000 h due to the impact of incidents. A list of the different failures during the test is provided in Table 2. Both types of incidents (fuel supply fluctuations and overloading failure of the electronic load) most probably lead to partial re-oxidation of the anode, accelerating the stack degradation toward 9500 h.

The goal of the present work being the investigation of cathode contamination by Cr, the cell least affected by the incidents on the anode side which could have damaged the sealing also is chosen here. Cell n° 5 with a voltage decay from 757 mV to 706 mV, i.e. a degradation rate below −0.7% per 1000 h, is therefore analyzed. Located on the top of the short-stack, this cell could also be most easily dismounted from the other stack components. The observation of all cells remaining intact after endurance testing at 73% fuel utilization and 0.5 A cm^{-2} positively highlights the mechanical integrity of the stack assembly. The choice of sample locations for the post-test analysis was done as follows.

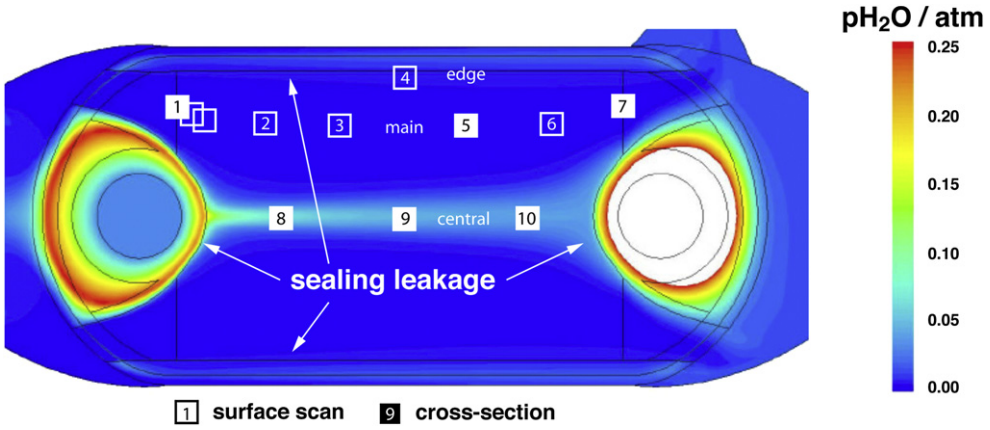

Fig. 4. The sealing leakage-caused water generation modeling result, as previously published by Z. Wuillemin [8], guides the post-test analyses; sample positions for surface scans are indicated by empty squares numbered 1–10; the full squares correspond to sample locations where cross-sections were investigated in addition; the larger size of post-test sample 1 enabled surface measurements on 3 consecutive positions along the air inlet channel (cf. Fig. 10) and the sample location is therefore indicated as tripled.

The modeling background for p(H_2O) and Cr-concentration distribution within this cell design depicted on Fig. 4 and further on in Fig. 9[B] is in-depth described elsewhere by Wuillemin [8]. These modeling results suggest sealing-proximal and air in-/out-let regions to be most prone to Cr-poisoning.

The cell dissection to obtain 10 samples distributed within the air flow field followed the guidance from these p(H_2O)-/Cr-distribution modeling results; the 10 samples extracted for surface analysis, comprising 6 samples also for subsequent cross-section study (locations 1, 5, 7, 8, 9, 10), were chosen along 3 air channels (named: edge, main and central, as illustrated in Fig. 4).

Energy-dispersive X-ray spectroscopy (EDS) surface scans were performed on 1 mm^2 regions on the 10 samples to obtain space-averaged Cr quantification, for which the measurement device and protocol are described elsewhere [10].

The 6 samples dedicated for cross-section studies followed embedding in epoxy medium, cutting with a diamond wire, polishing with diamond lapping films and carbon coating steps, before EDS analysis. The acquisition parameters, previously described [11], were tuned toward high acceleration voltage to provoke high excitation of the Cr K-line emission needed for proper Cr quantification, and toward high count rates, enabling the collection of statistically senseful data within reasonable measurement time.

Table 1
Summary of stack performance and degradation evolution after ca. 10,000 h operation; area specific, ohmic and polarization resistances (ASR, R_{Ohmic} and $R_{Polarization}$, respectively) are averaged values over the 5-cell stack; values for each individual cell (including the best performing cell n° 5, dealt with in this study) are also given. The monitoring description, via impedance spectroscopy, is given by Comminges et al. in a previous work [1].

Recorded parameter	Unit	Value		Variation (%)
		0 h	9630 h	
Stack temperature	°C	756	753	−0.4
Current density	A cm^{-2}	0.5	0.5	–
Fuel utilization	%	73	–	–
Stack voltage	V	3.752	3.241	−13.6
Stack ASR (at 0.5 A cm^{-2})	Ω cm^2	0.56	0.76	+35.7
Stack R_{Ohmic}	Ω cm^2	0.18	0.36	+100
Stack $R_{Polarization}$	Ω cm^2	0.38	0.4	+5.3
Cell 5 voltage	mV	757	706	−6.7
Cell 4 voltage	mV	747	646	−13.5
Cell 3 voltage	mV	753	657	−12.7
Cell 2 voltage	mV	762	624	−18.1
Cell 1 voltage	mV	754	627	−16.8

The Cr profiles depicted on Figs. 5[B] and 6 were generated by transforming qualitative 2D EDS maps into quantitative 1D elemental/phase profiles [12], by space-averaging EDS data over thin cathode slices.

3. Results and discussion

3.1. Cr profile in LSCF

An objective Cr-poisoning picture independent of the investigator's eye [13] was obtained by systematically drawing elemental and phase profiles through the complete cathode thickness. Fig. 5 [A] illustrates the cathode layers assembly from left to right: (i) a current collection layer (CL) made of (sub)micron LSCF grains, (ii) a functional cathode layer (FL) comprising a fraction of bulky CGO grains (light gray contrast) and (iii) a CGO buffer layer (BL). The phase profiles, with decreasing LSCF and increasing ceria contents toward the cathode/electrolyte interface, enable the CL/FL/BL assembly to be correctly identified. The LSCF and CGO phase fractions are obtained by adding to the sum of the metallic elements the corresponding oxygen amounts, i.e. $O_{LSCF} = 3/2\Sigma_{La,Sr,Co,Fe}$ and $O_{CGO} = 2\Sigma_{Ce,Gd}$ (+3 oxidation state in CGO neglected as approximation), prior to normalization.

The elemental Cr profile shown in Fig. 5[B] (EDS Cr data taken from the central sample location 9) comprises two regimes of Cr accumulations in the CL and FL, respectively. A preferential distribution of Cr accumulations near the gas–CL interface, with decreasing amounts toward the FL–electrolyte interface, is observed; this was previously found by others for LSCF-based cathodes [2]. This result alone, quantified for sample location 9, only qualitatively represents the Cr-poisoning-caused contaminant distribution in a complete LSCF-cathode cross-section; multiple measurements are needed to holistically depicture Cr-poisoning within the cell.

Table 2
Description of the failures observed during the long-term test.

Time (h)	Description of the incident
4533	Fluctuations of hydrogen flow rate
6535	Fluctuations of hydrogen flow rate
6660	Fluctuations of hydrogen flow rate
8587	Load failure, increase of current
9470	Cell n° 1 and n° 4 voltages started to decrease

Reprinted with permission from Ref. [1].

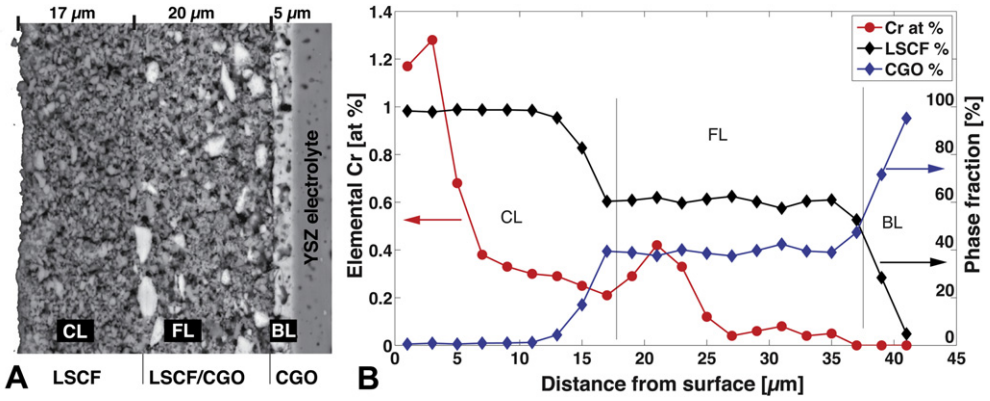

Fig. 5. [A] SEM micrograph of SOFC cross-section showing from left to right the LSCF collector layer (CL), the LSCF–CGO functional layer (FL), a CGO buffer layer (BL), and the YSZ electrolyte; [B] LSCF and CGO phase profiles with increasing CGO-content toward the cathode/electrolyte interface; Cr profile through the cathode thickness (location 9) reveals two trends: i) in the CL with decreasing amounts from the surface inwards ii) in the FL with again higher amounts than in the FL-proximal CL region.

3.2. Cr deposition mechanisms in LSCF-based cathodes

Elemental Cr profiles for the 6 cross-section samples (locations 1, 5, 7, 8, 9, 10) are presented in Fig. 6. Differences in amounts and distributions of Cr are found for the different sample positions along the air flow and across the cell width. A characteristic Cr distribution through the LSCF-cathode thickness, illustrated in Fig. 7, is obtained by averaging the profiles of Cr amounts, normalized with respect to the most contaminated zone, i.e. the gas–CL interface.

Decreasing Cr amounts in the current collector with fairly constant values in the FL indicate a combination of Cr deposition mechanisms, suggested by others [14,15] driven both by the electrochemical activity (in cathode regions where the oxygen reduction process occurs) and the chemical reactivity (throughout the whole cathode thickness) of this mixed-conducting LSCF-based cathode. This is schematically illustrated on Fig. 8.

On the one hand, the main part of Cr-poisoning in LSCF cathodes is caused by the chemical reactivity of SrO with Cr vapors to form $SrCrO_4$ [2], i.e. by the chemically-driven Cr deposition. Starting from the gas–CL interface, a decreasing Cr deposition rate through the whole LSCF-containing cathode thickness, caused by gas diffusion limitations, is therefore expected. On the other hand, when assuming that the electrochemically active cathode region is confined to the FL (Lu et al. [16] recently suggested LSCF cathodes to be active only within ca. 13 μm thickness), a polarization-driven Cr deposition rate only increasing toward the FL–electrolyte interface is expected. The electrochemically-driven Cr deposition mainly involves a reduction of Cr^{6+} vapor species into Cr^{3+} oxides at near-interface regions where the pO_2 is low.

Fig. 8 indicates schematically the combination of both decreasing (from the gas–CL interface) and increasing (toward the FL–electrolyte interface) contributions to correlate with the experimentally observed constant Cr profile within the FL. The shape of both the chemically and electrochemically-driven Cr deposition profiles relay on previous experimental results [4].

3.3. Cr-poisoning distribution within the cell

Fig. 9 depicts the severity of Cr-poisoning judged from surface analysis (the first microns from the LSCF surface are quantified) along three air flow channels, i.e. along the edge (location 4), within the main cell part (locations 1, 2, 3, 5, 6, 7) and in the center of the cell (locations 8, 9, 10). As the flow field is constricted at the air in-/out-let regions (cf. Fig. 1), these areas count as a single entry zone, split into three flow lines (main, edge and central) between inlet and outlet.

The highest Cr amounts are measured at the air inlet region (location 1), indicating the air flow feed to the cathode compartment to be loaded with Cr vapor species, hence pointing to Cr sources located upstream of the cell. The strongly decreased Cr

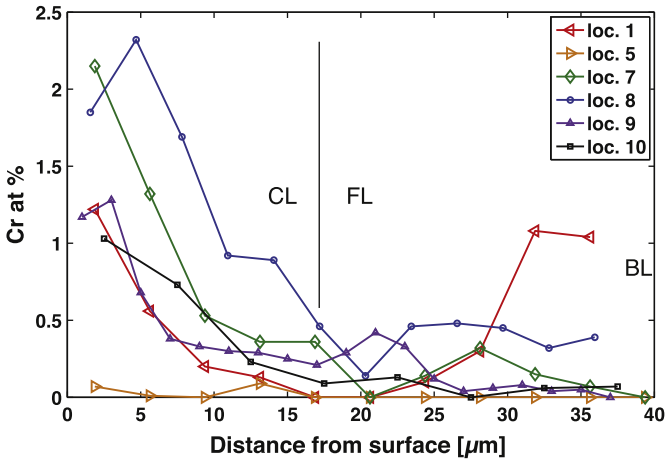

Fig. 6. Six Cr profiles across the cathode thickness reveal differences in severity (amounts) and shape (distribution) of Cr accumulations.

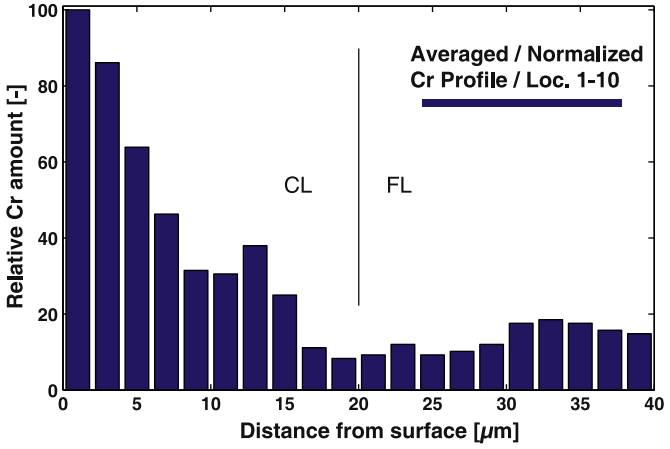

Fig. 7. Distribution of Cr accumulation, averaged on normalized profiles for sample locations 1, 5, 7, 8, 9, 10, through the cathode thickness: decreasing amounts in the CL and approximately constant severity within the FL is observed.

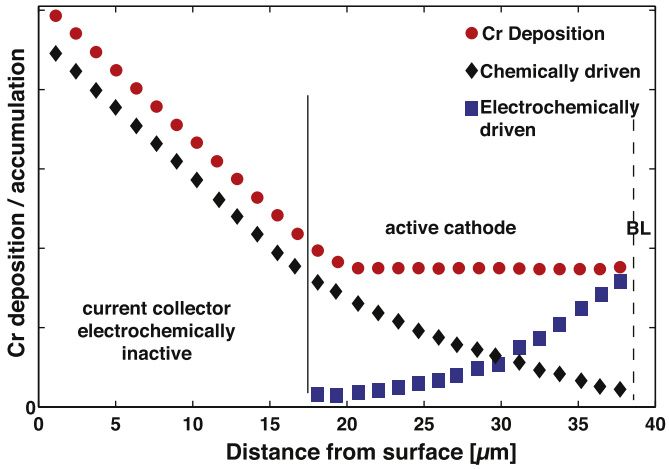

Fig. 8. The present work suggests the observed profile (dots – cf. Fig. 7) to result from a combination of electrochemical activity near the FL–electrolyte interface due to oxygen depletion toward this interface (squares), with chemical surface reactivity within the entire cathode thickness (diamonds).

amounts along the air channels (locations 2, 3, 5, 6), with respect to the inlet location 1, suggest more Cr is being trapped by the LSCF CL surface than is being generated by the MIC.

The main part of the cell (locations 2, 3, 5, 6) remains very low in Cr-poisoning, with slightly increasing amounts toward the air outlet. The protective solutions on the MIC to prevent Cr vapor emanation with an Mn/Co/Fe barrier coating in combination with the GDL thus appear to be sufficient for the time being for these operating conditions. This can in particular be brought into correlation with the measured increase in average polarization resistance of only 0.02 Ω cm^2 for nearly 10,000 h (cf. Table 1), which translates to less than 0.4%/1000 h ASR increase due to polarization; moreover, this ASR increase accounts for all cathode and anode contributions combined, of which the Cr contamination is only one process.

The cathode regions close/downstream the sealing locations along the cell edge flow (locations 1, 4, 7) and the central flow (locations 8, 9, 10) reveal higher Cr amounts (>1 atomic %). These observations correlate with the model predictions for H_2O and Cr generation illustrated in Figs. 4 and 9[B]. The preferential Cr accumulation at sealing-proximal locations corroborates that H_2 fuel partly leaks through the sealing to generate steam and subsequently $CrO_2(OH)_2$ vapor in the cathode compartment, to aggravate Cr-poisoning.

A direct link to cathode degradation is difficult to establish, since measurements on a greater extent of sample locations across the cell width would be needed to determine the proportion of high/low poisoned cathode regions. Moreover, to generate a link to degradation, spatially-resolved degradation data (not recorded here) would be a likewise prerequisite to locally-resolved contamination assessment, as the local degradation differs from global degradation in SOFC [17].

Absolute and direct correlations, such as Cr concentration [Cr μg cm^{-2}] versus voltage decay [-%/time] were reported before in button cell test investigations [12,18], but cannot be extracted from the present work, as the test in stack configuration superimposes other degradation effects, not limited to Cr-poisoning alone.

3.4. Superimposed degradation

Besides Cr-poisoning and other well-identified degradation phenomena such as zirconate formation [19] this work aims to shed light on the effect of the following:

i) Fig. 4 having predicted differences in the local water vapor pressure according to the position within the cell, the effect of p(H_2O) alone on LSCF-based cathode behavior (without interference from Cr) should be discussed. Literature shows high uncertainty among different authors [20–25], reported in Table 3, where statements for (La,Sr)MnO_3 (LSM)-based cathodes are included for comparison purpose. The observations in our present work do not enable, either, to give a direct correlation between water vapor and cathode degradation, other than illustrating a p(H_2O)-dependent aggravation of the Cr-poisoning phenomenon [6].

ii) After 10,000 h SOFC operating time, the SO_2 content (in ppb range in environmental air fed to the cathode) is expected to lead to secondary phase formation upon reaction with LSCF-based cathode, as recently reported by Wang et al. [26]; i.e. $SrSO_4$ formation occurs when LSCF is exposed to SO_2. Indeed, also in our work Fig. 10 identifies S contamination at the air inlet region of the cell (sample location 1), besides Cr. The EDS analysis shown in Fig. 11 of a single grain of contamination accumulation (within the limitations of SEM-EDS analysis) suggests a combined Cr/S-strontium oxide to be formed in these combined contaminating conditions, as recently reported for LSC- and LSM-based cathodes [27,28].

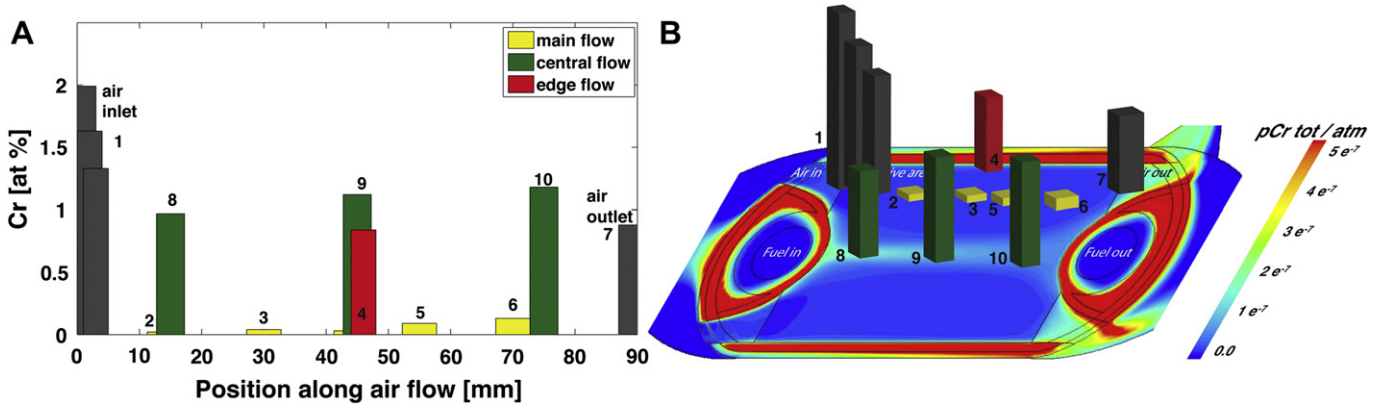

Fig. 9. [A] Cr amounts determined by EDS scans on 1 mm^2 LSCF surface regions; [B] schematic representation of preferential Cr accumulations at the air inlet and sealing-proximal cathode locations, superimposed to a model prediction of Cr generation; predictions of fuel sealing leakage with associated steam production and subsequent Cr-oxyhydroxide generation in the cathode compartment are confirmed by the locally measured Cr amounts.

Table 3
Literature data shows an unclear effect of water vapor alone on LSCF-based cathodes; a similar picture can be drawn for (La,Sr)MnO_3, given here for comparison.

Author ref.	Cathode type 1	Cathode type 2	Condition (T, p(H_2O))
J. Guan et al. [20]	LSCF: unclear	LSM/YSZ: no effect	800 °C, 3%
A. Hagen et al. [21]	–	LSM/YSZ: partially reversible LSM/YSZ-optimized: stable performance	750–850 °C, 4%
X. Chen et al. [22]	–	LSM: no effect	900 °C, 3%
R.R. Liu et al. [23]	LSCF: stable short-term, long-term decomposition	LSM: gradual irreversible decomposition	800 °C, 3–20%
J. Nielsen et al. [24]	LSCF/CGO: tolerance/no effect	LSM/YSZ: passivation degradation	750 °C, <13%
E. Bucher et al. [25]	LSCF: oxygen reduction activity decrease	–	600–700 °C, 30–75 RH

3.5. Solutions for Cr-poisoning mitigation

The overall air electrode pollution, in this combination of LSCF-based cathode and MnCoFe-protected MIC, remains relatively low, indicating the layer's assembly materials choice to be possible; the Cr-poisoning degradation phenomenon alone does not seem to preclude this cell to reach 40,000 h operation (when considering that other degradation phenomena have contributed to the overall observed −1.4%/1000 h stack voltage decay, predominantly by ohmic degradation). Nevertheless, since Cr contamination has been revealed after 9630 h operation, the following points are open for possible mitigation of the extent of Cr-poisoning for future developments:

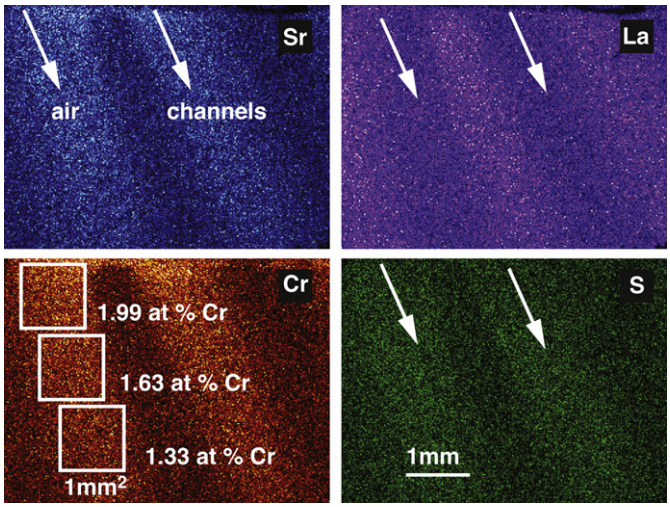

Fig. 10. SEM-EDS elemental maps on air channels at the air inlet location, with Cr quantification on three 1 mm^2 regions at location 1 (cf. Figs. 4 and 9), indicate upstream-generated Cr/S pollution to decrease along the air flow.

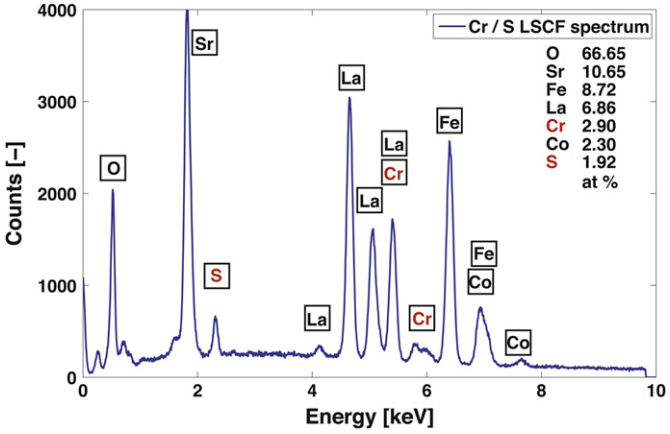

Fig. 11. EDS spectrum of a single grain of contamination accumulation reveals the formation of an S-added Sr-chromate phase upon combined Cr/S-poisoning of LSCF.

i) Cathode material. Regarding Cr-poisoning, the LSCF cathode presents a senseful tradeoff between cathodes prone to mainly surface reaction, as for (La,Sr)CoO_3 (LSC) [4], or those prone to mainly electrochemical-driven deposition like LSM [12]. In LSC-based cathode materials, densified and bulky $SrCrO_4$ grains are formed on the electrode surface, leading to conductivity and diffusion limitations as well as possible spallations of adjacent cathode layers (higher thermal expansion coefficient for $SrCrO_4$) [28], caused by the high Sr activity in LSC. LSM cathodes, although presenting the lowest Sr activity and hence the lowest reactivity with Cr vapors for La/Sr-based perovskite compositions, suffer from the most severe case of Cr-poisoning, i.e. polarization-induced MnO-driven Cr deposition on electrochemically active cathode triple-phase-boundaries, blocking the oxygen reduction reaction. Alternative Mn/Sr free cathode compositions, like (La)(Ni,Fe)O_3 (LNF), supposedly Cr-tolerant [29,30], suffer likewise from Cr deposition mechanisms, both electrochemically- and chemically-driven as demonstrated by others [31,32]. A choice left to mitigate the impact of Cr-poisoning might be the increase of the CL thickness to trap Cr in the current collector before reaching electrochemically active cathode regions.

ii) MIC barrier coating. Since the main part of the cell experienced only small Cr-poisoning, and as the Cr concentration was decreasing faster by LSCF trapping in air inlet regions than the amounts generated by the cathode-proximal MIC, only limited improvement is expected with further protective solutions on the MIC.

iii) Balance-of-plant (BoP) components. More improvement is expected by decreasing the Cr load, generated by Cr sources located upstream the cell, of the air inlet flow. It is, however, unreasonable to protect the complete surface of complex-shaped system parts of the BoP, which represents in volume the larger part of an SOFC system. More pragmatic is the implementation of an air-filtering material, acting as chemical trap for Cr vapors generated by upstream system components [33].

iv) Sealing materials. Most improvement is expected by decreasing the amount of hydrogen leakage from the anode side into the cathode compartment by perfecting the sealing. Tighter sealing would decrease the water vapor pressure over large parts of the cathode compartment, and therefore mitigate the p(H_2O)-dependent aggravation of Cr-poisoning.

4. Conclusion

In this work, we systematically applied an objective quantification methodology to picture the severity of Cr-poisoning in an

LSCF cathode-based SOFC stack after 10,000 h operation. This approach, combined to the modeling prediction of Cr distribution given by local p(H_2O)-dependent Cr generation and deposition, allowed the effect and causes of Cr-poisoning to be identified, leading to recommendations for Cr-poisoning mitigation and lifetime improvement.

Acknowledgments

This work was supported by the Swiss SOF-CH-ASE project, cofunded by the Swiss Federal Energy Office (BFE) and swiss*electric* research. Danièle Laub, Brigitte Greenwood and Nicola Accardo are warmly thanked for experimental work.

References

[1] C. Comminges, Q. Fu, M. Zahid, N. Yousfi Steiner, O. Bucheli, Electrochim. Acta 59 (2012) 367.
[2] N.H. Menzler, P. Batfalsky, S.M. Gross, V. Shemet, F. Tietz, ECS Trans. 35 (2011) 195.
[3] J.A. Schuler, C. Gehrig, Z. Wuillemin, A.J. Schuler, J. Wochele, C. Ludwig, A. Hessler-Wyser, J. Van herle, J. Power Sources 196 (2011) 7225.
[4] J.A. Schuler, A.J. Schuler, Z. Wuillemin, A. Hessler-Wyser, C. Ludwig, J. Van herle, ECS Trans. 35 (2011) 2001.
[5] O. Thomann, M.H. Pihlatie, J.A. Schuler, O. Himanen, J. Kiviaho, Electrochem. Solid-State Lett. 15 (2012) B35.
[6] K. Hilpert, D. Das, M. Miller, D.H. Peck, R. Weiss, J. Electrochem. Soc. 143 (1996) 3642.
[7] Z. Wuillemin, N. Autissier, A. Nakajo, M. Luong, J. Van herle, D. Favrat, J. Fuel, Cell. Sci. Technol. 5 (2008) 1.
[8] Z. Wuillemin, EPFL thesis no. 4525, 2009.
[9] H. Yokokawa, ECS Trans. 35 (2011) 207.
[10] J.A. Schuler, Z. Wuillemin, A. Hessler-Wyser, J. Van herle, Electrochem. Solid-State Lett. 14 (2011) B20.
[11] J.A. Schuler, P. Tanasini, A. Hessler-Wyser, J. Van herle, Scr. Mater. 63 (2010) 895.
[12] J.A. Schuler, P. Tanasini, A. Hessler-Wyser, C. Comninellis, J. Van herle, Electrochem. Commun. 12 (2010) 1682.
[13] M. Ananyev, A. Gavrilyuk, D. Bronin, R. Steinberger-Wilckens, J. Mertens, in: EFCF Proceeding B04, 2011, p. 21.
[14] T. Horita, H. Kishimoto, K. Yamaji, M.E. Brito, T. Shimonosono, D. Cho, M. Izuki, F. Wang, H. Yokokawa, ECS Trans. 35 (2011) 511.
[15] X. Chen, L. Zhang, E. Liu, S.P. Jiang, Int. J. Hydrogen Energy 36 (2011) 805.
[16] Z. Lu, J. Hardy, J. Templeton, J. Stevenson, J. Power Sources 198 (2012) 90.
[17] Z. Wuillemin, A. Nakajo, A. Müller, J.A. Schuler, S. Diethelm, J. Van herle, D. Favrat, ECS Trans. 25 (2009) 457.
[18] M. Krumpelt, T.A. Cruse, B.J. Ingram, J.L. Routbort, S. Wang, P.A. Salvador, G. Chen, J. Electrochem. Soc. 157 (2010) B228.
[19] A. Hessler-Wyser, Z. Wuillemin, J.A. Schuler, A. Faes, J. Van herle, J. Mater. Sci. 46 (2011) 4532.
[20] J. Guan, S. Zecevic, Y. Liu, P. Lam, R. Klug, M. Alinger, S. Taylor, B. Ramamurthi, R. Sarrafi-Nour, S. Renou, ECS Trans. 7 (2007) 405.
[21] A. Hagen, M. Chen, K. Neufeld, Y.L. Liu, ECS Trans. 25 (2009) 439.
[22] X. Chen, Y. Zhen, J. Li, S.P. Jiang, Int. J. Hydrogen Energy 35 (2010) 2477.
[23] R.R. Liu, S.H. Kim, S. Taniguchi, T. Oshima, Y. Shiratori, K. Ito, K. Sazaki, J. Power Sources 196 (2011) 7090.
[24] J. Nielsen, A. Hagen, Y.L. Liu, Solid State Ionics 181 (2010) 517.
[25] E. Bucher, A. Egger, M. Yang, W. Sitte, in: EFCF Proceeding 0702, 2010, p. 1.
[26] F. Wang, K. Yamaji, D.-H. Cho, T. Shimonosono, H. Kishimoto, M.E. Brito, T. Horita, H. Yokokawa, J. Electrochem. Soc. 158 (2011) B1391.
[27] J.A. Schuler, Z. Wuillemin, A. Hessler-Wyser, J. Van herle, ECS Trans. 25 (2009) 2845.
[28] J.A. Schuler, H. Yokokawa, C.F. Calderone, Q. Jeangros, Z. Wuillemin, A. Hessler-Wyser, J. Van herle, J. Power Sources 201 (2012) 112.
[29] T. Komatsu, Y. Yoshida, K. Wantanabe, R. Chiba, H. Taguchi, H. Orui, H. Arai, J. Power Sources 195 (2010) 5601.
[30] Y. Yoshida, R. Chiba, T. Komatsu, M. Yokoo, K. Hayashi, H. Orui, H. Arai, ECS Trans. 35 (2011) 2313.
[31] M.K. Stodolny, B.A. Boukamp, F.P.F. van Berkel, ECS Trans. 35 (2011) 2035.
[32] J.A. Schuler, H. Luebbe, A. Hessler-Wyser, J. Van herle, J. Power Sources, in press.
[33] J.A. Schuler, A.J. Schuler, D. Penner, A. Hessler-Wyser, C. Ludwig, J. Van herle, Electrochem. Solid-State Lett. 14 (2011) B132.